

# Single hole dynamics in the one dimensional $t$ - $J$ model

Michael Brunner, Fakhre F. Assaad and Alejandro Muramatsu

*Institut für Theoretische Physik III, Universität Stuttgart, Pfaffenwaldring 57, D-70550 Stuttgart,  
Federal Republic of Germany*

(August 11, 2018)

We present a new finite-temperature quantum Monte Carlo algorithm to compute imaginary-time Green functions for a single hole in the  $t$ - $J$  model on non-frustrated lattices. Spectral functions are then obtained with the Maximum Entropy method. Simulations of the one-dimensional case show that a simple charge-spin separation *Ansatz* is able to describe the overall features of the spectral function over the whole energy range for values of  $J/t$  from  $1/3$  to  $4$ . This includes the bandwidth  $W \sim 4t + J$  and the compact support of the spectral function. The quasiparticle weight  $Z_k$  is computed on lattices up to  $L = 96$  sites, and scales as  $Z_k \propto L^{-1/2}$ .

Understanding single hole dynamics in quantum antiferromagnets is a decisive step towards a comprehensive description of elementary excitations in strongly correlated systems. Experimental realizations are found in compounds such as  $SrCuO_2$  [1],  $Na_{0.96}V_2O_5$  [2] for chains,  $Sr_{14}Cu_{24}O_{41}$  [3] for ladders and  $Sr_2CuO_2Cl_2$  [4] for planes. In particular chain compounds attract at present an increasing amount of interest in order to elucidate, whether signals of charge-spin separation as predicted from Luttinger-liquid theory can be observed experimentally. On the other hand, theoretical treatments based on Bethe-*Ansatz* (BA) results lead recently to a complete description of the spectral function of the Hubbard model at  $U = \infty$  [5] and the low energy sector in the nearest-neighbour (NN)  $t$ - $J$  model, where explicit results are obtained at the supersymmetric (SuSy) point [6]. Further exact results - apart from exact diagonalizations which suffer from strong finite-size effects - are available only for the inverse-square exchange (ISE) [7]  $t$ - $J$  model at the SuSy point. In order to be able to compare with experiments, it is crucial to extend such studies to realistic values of the parameters and possibly beyond the asymptotic low energy limit.

In this letter, we present a simple finite-temperature quantum Monte Carlo (QMC) algorithm capable of dealing with this issue for the NN  $t$ - $J$  model. For single-hole excitations and in the absence of frustration, the method is free of the notorious sign problem, and applicable to chains, n-leg ladders and planes. Here, we concentrate on chains. Our simulations lead to the conclusion that the overall features of the spectral functions are well described by a charge-spin separation *Ansatz* (CSSA) based on a mean-field slave-boson picture [9], where the hole spectral function is given by the convolution of the spectral functions of free holons and spinons. The agreement with the simulations is obtained over all energy scales

and values of  $J/t$  ranging from  $1/3$  to  $4$ . At the SuSy point a more detailed understanding of the spectrum is achieved by supplementing the simple model with BA results. A finite-size scaling on chains up to  $L = 96$  sites shows that the quasi-particle weight  $Z_k$  vanishes as  $1/\sqrt{L}$ , a result which was beyond numerical capabilities up to now.

Our starting point is the NN  $t$ - $J$  model,

$$H_{t-J} = -t \sum_{\langle i,j \rangle, \sigma} \tilde{c}_{i,\sigma}^\dagger \tilde{c}_{j,\sigma} + J \sum_{\langle i,j \rangle} \left( \vec{S}_i \cdot \vec{S}_j - \frac{1}{4} \tilde{n}_i \tilde{n}_j \right). \quad (1)$$

Here  $\tilde{c}_{i,\sigma}^\dagger$  are projected fermion operators  $\tilde{c}_{i,\sigma}^\dagger = (1 - c_{i,-\sigma}^\dagger c_{i,-\sigma}) c_{i,\sigma}^\dagger$ ,  $\tilde{n}_i = \sum_\alpha \tilde{c}_{i,\alpha}^\dagger \tilde{c}_{i,\alpha}$ ,  $\vec{S}_i = (1/2) \sum_{\alpha,\beta} c_{i,\alpha}^\dagger \vec{\sigma}_{\alpha,\beta} c_{i,\beta}$ , and the sum runs over nearest neighbours. After a canonical transformation this model is cast into the form [10]

$$\tilde{H}_{t-J} = +t \sum_{\langle i,j \rangle} P_{ij} f_i^\dagger f_j + \frac{J}{2} \sum_{\langle i,j \rangle} \Delta_{ij} (P_{ij} - 1), \quad (2)$$

where  $P_{ij} = (1 + \vec{\sigma}_i \cdot \vec{\sigma}_j)/2$ ,  $\Delta_{ij} = (1 - n_i - n_j)$  and  $n_i = f_i^\dagger f_i$ . In this mapping, one uses the following identities for the standard creation ( $c_{i,\sigma}^\dagger$ ) and annihilation ( $c_{i,\sigma}$ ) operators  $c_{i\uparrow}^\dagger = \gamma_{i,+} f_i - \gamma_{i,-} f_i^\dagger$ ,  $c_{i\downarrow}^\dagger = \sigma_{i,-} (f_i + f_i^\dagger)$ , where  $\gamma_{i,\pm} = (1 \pm \sigma_{i,z})/2$  and  $\sigma_{i,\pm} = (\sigma_{i,x} \pm i\sigma_{i,y})/2$ . The spinless fermion operators fulfill the canonical anticommutation relations  $\{f_i^\dagger, f_j\} = \delta_{i,j}$ , and  $\sigma_{i,a}$ ,  $a = x, y$ , or  $z$  are the Pauli matrices. The constraint to avoid doubly occupied states transforms to the conserved and holonomic constraint  $\sum_i \gamma_{i,-} f_i^\dagger f_i = 0$ .

The Green function in the spin up sector may be written as

$$G_\uparrow(i-j, \tau) = \langle T \tilde{c}_{i,\uparrow}(\tau) \tilde{c}_{j,\uparrow}^\dagger \rangle = \langle T f_i^\dagger(\tau) f_j \rangle \quad (3)$$

where  $T$  corresponds to the time ordering operator. Inserting complete sets of spin states the quantity above transforms as

$$\begin{aligned} -G(i-j, -\tau) &= \frac{\sum_{\sigma_1} \langle v | \otimes \langle \sigma_1 | e^{-(\beta-\tau)\tilde{H}_{t-J}} f_j e^{-\tau\tilde{H}_{t-J}} f_i^\dagger | \sigma_1 \rangle \otimes | v \rangle}{\sum_{\sigma_1} \langle \sigma_1 | e^{-\beta\tilde{H}_{t-J}} | \sigma_1 \rangle} = \\ &= \sum_{\vec{\sigma}} P(\vec{\sigma}) \times \frac{\langle v | f_j e^{-\Delta\tau\tilde{H}(\sigma_n, \sigma_{n-1})} e^{-\Delta\tau\tilde{H}(\sigma_{n-1}, \sigma_{n-2})} \dots e^{-\Delta\tau\tilde{H}(\sigma_2, \sigma_1)} f_i^\dagger | v \rangle}{\langle \sigma_n | e^{-\Delta\tau\tilde{H}_{t-J}} | \sigma_{n-1} \rangle \dots \langle \sigma_2 e^{-\Delta\tau\tilde{H}_{t-J}} | \sigma_1 \rangle} + \mathcal{O}(\Delta\tau^2) \\ &= \sum_{\vec{\sigma}} P(\vec{\sigma}) G(i, j, \tau, \vec{\sigma}) + \mathcal{O}(\Delta\tau^2) \end{aligned} \quad (4)$$

Here  $m\Delta\tau = \beta$ ,  $n\Delta\tau = \tau$ ,  $\Delta\tau t \ll 1$  and  $\exp(-\Delta\tau\tilde{H}(\sigma_1, \sigma_2))$  is the evolution operator for the holes, given the spin configuration  $(\sigma_1, \sigma_2)$ . In the case of single hole dynamics  $|v\rangle$  is the vacuum state for holes, and  $P(\vec{\sigma})$  is the probability distribution of a Heisenberg antiferromagnet for the configuration  $\vec{\sigma}$ , where  $\vec{\sigma}$  is a vector containing all intermediate states  $(\sigma_1, \dots, \sigma_n, \dots, \sigma_m, \sigma_1)$ . The sum over spins is performed in a very efficient way by using a

world-line cluster-algorithm [11]. As the evolution operator for the holes is a bilinear form in the fermion operators,  $G(x, \tau, \vec{\sigma})$  can be calculated exactly.  $G(x, \tau, \vec{\sigma})$  contains a sum over all possible fermion paths between  $(i, 0)$  and  $(j, \tau)$ , where  $i - j = x$ . This stands in contrast to the worm approach [12], where fermion paths are sampled stochastically. The numerical effort to calculate  $G(x, \tau, \vec{\sigma}) \forall x, \tau$  scales as  $L\tau$ . Spectral properties are obtained by inverting the spectral theorem

$$G(k, \tau) = \int_{-\infty}^{\infty} d\omega A(k, \omega) \frac{\exp(-\tau\omega)}{\pi(1 + \exp(-\beta\omega))} \quad (5)$$

with the Maximum Entropy method (MEM) [13]. Since  $P(\vec{\sigma})$  is the probability distribution for the quantum antiferromagnet, the algorithm does not suffer from sign problems on bipartite lattices and next neighbour interactions in any dimension. However, when the spin and charge dynamics evolve according to very different time scales ( $J \lesssim 0.2t$ ),  $G(x, \tau, \vec{\sigma})$  shows an increasing variance. Best results are obtained at the SuSy point and an appreciable range of  $J/t$  may be considered as shown below.

We now concentrate on the one-dimensional  $t$ - $J$  model. The simulations were performed at temperatures  $T \leq \min(J, t)/15$ , such that no appreciable changes with a further decrease in temperature can be seen: the results correspond to the zero temperature limit, a limit which is in general difficult to reach in other finite-temperature fermionic algorithms. We compare our results with the predictions of the CSSA, where free holons and spinons are described by [9,14]

$$H = -\frac{t_h}{2} \sum_{\langle i,j \rangle} h_i^\dagger h_j - \frac{J_s}{2} \sum_{\langle i,j \rangle} s_{i,\sigma}^\dagger s_{j,\sigma}. \quad (6)$$

Here the electron operator  $c_{i,\sigma}$  is given by the product of a holon ( $h_i$ ) and a spinon ( $s_{i,\sigma}$ ) operator,  $c_{i\sigma} = s_{i,\sigma} h_i^\dagger$ , the holon being a boson and the spinon a spin-1/2 fermion. As a consequence of the above *Ansatz*, the dispersion relations of the free holons and spinons are given by  $\epsilon_h = -t_h \cos q_h$  and  $\epsilon_s = -J_s \cos q_s$  respectively, whereas the energy of the hole is  $E(k) = \epsilon_h - \epsilon_s$  and by momentum conservation  $k = q_h - q_s$ . We take  $t_h$  and  $J_s$  as two free parameters in contrast to a mean-field approximation, where they have to be calculated self-consistently. The spectral function is then given by a convolution of the spinon and holon Green functions. The lowest attainable energy ( $-t_h$ ) and highest one ( $t_h + J_s$ ) define the bandwidth of the hole,  $2t_h + J_s$ . Since the full band-width obtained by considering the compact support of the spectral function at  $J = 0$  is known to be exactly  $4t$  [5], we take  $t_h = 2t$ . In order to determine  $J_s$ , we consider the overall bandwidth, as obtained from the simulation. As can be seen in Fig. 1, for all values of  $J$ ,

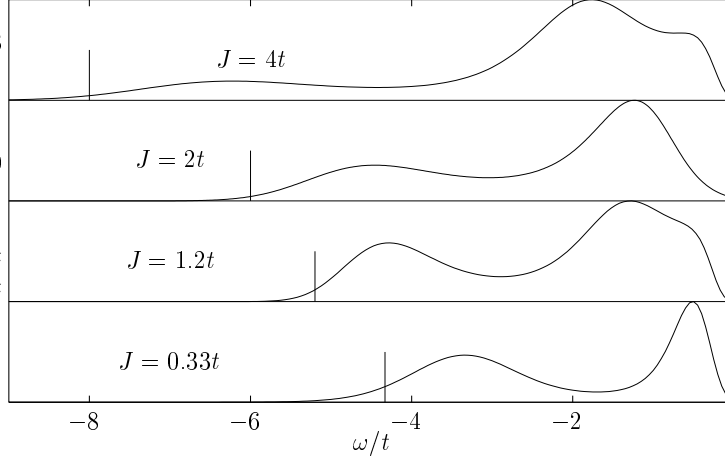


FIG. 1. Density of states  $N(\omega)$  for different values of  $J/t$ . The vertical line indicates  $4t + J$ .

the width of the density of states  $N(\omega)$  scales approximately as  $4t + J$  in the parameter range considered, leading to  $J_s = J$ .

Beyond predicting bandwidths, the CSSA describes accurately the support of the spectral function in the case  $J = 0$ , when compared with exact results [5,9]. If furthermore phase string effects [9] are taken into account, the singularities of  $A(k, \omega)$  related to holons and spinons can be reproduced. For finite  $J$ , the minimal (maximal) possible energy of a hole in CSSA is given by  $E(k) = -F_k$  ( $E(k) = F_k$ ) for  $k < k_0$  ( $k > k_0$ ), where  $F_k \equiv \sqrt{J^2 + 4t^2 - 4tJ \cos(k)}$  contains both holon and spinon contributions, and  $k_0$  is determined by  $\cos(k_0) = J/(2t)$ . The remaining parts of the compact support are given by  $E(k) = \mp 2t \sin(k)$  for  $k > k_0$  (lower edge) and  $k < k_0$  (upper edge) respectively. Such dispersions correspond to holons with momentum  $k + q_s$ , and a spinon with  $q_s = \mp \pi/2$  [6,9]. As  $J \rightarrow 2t$ ,  $k_0 \rightarrow 0$  and the lower edge of the compact support is entirely determined by the dispersion of the holon.

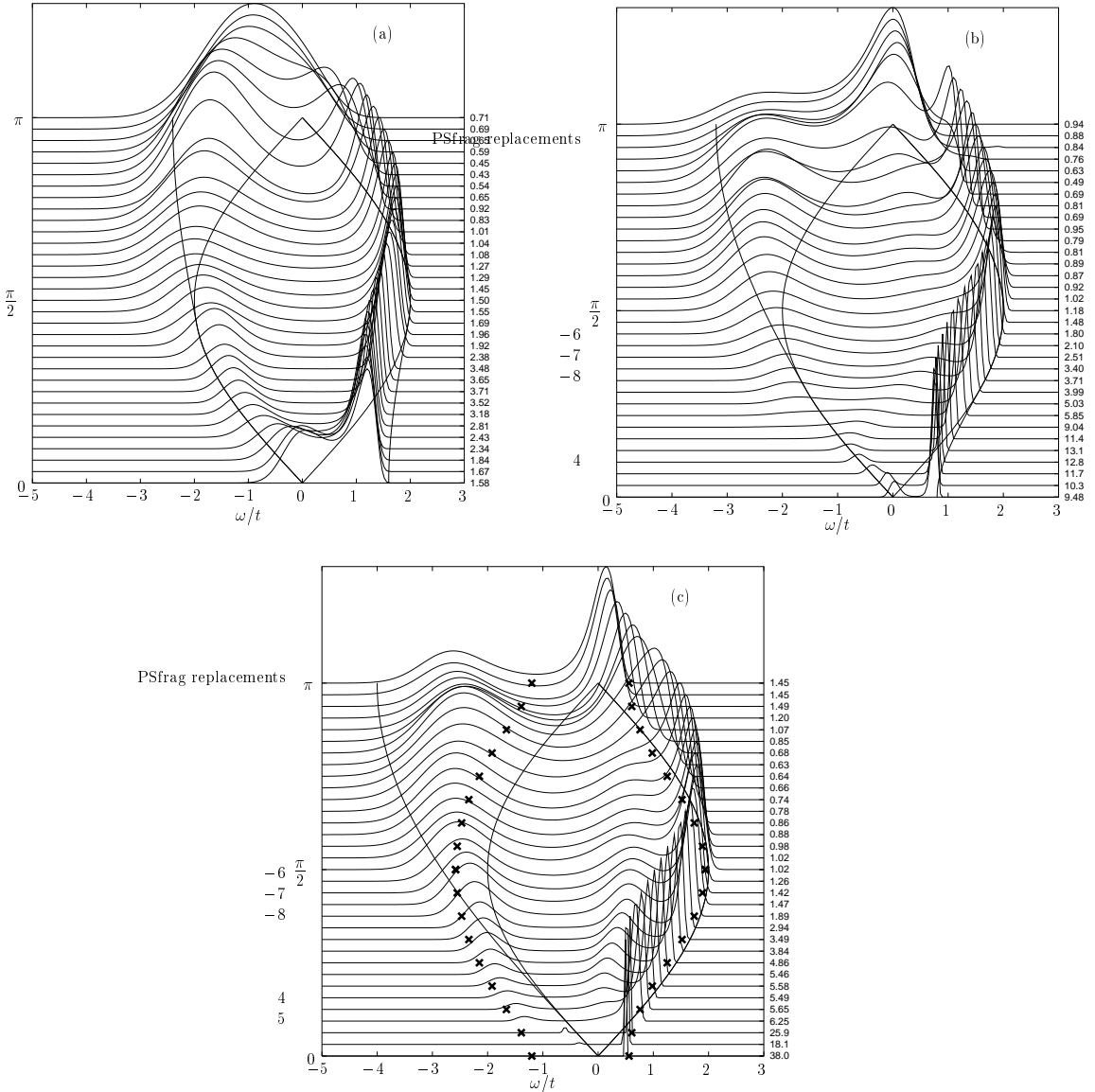


FIG. 2. Spectral function  $A(k, \omega)$  for  $J = 0.4t$  (a),  $J = 1.2t$  (b) and  $J = 2t$  (c). Here the wave vector  $k \in [0, \pi]$  is given on the y-axis. For clarity, the data is rescaled by the number given at the right hand side of the plot. Further details are discussed in the text.

We now compare the above predictions with our QMC data. Figure 2 shows  $A(k, \omega)$  for  $J/t = 0.4$  (a), 1.2 (b) and 2 (c). In all cases the compact support is reproduced very well by the CSSA. The *Ansatz* also predicts singularities at the lower (upper) edge for  $k < k_0$  ( $k > k_0$ ), and when phase strings are considered [9] along the edges and the holon lines ( $\pm 2t \sin(k)$ ) for all momenta. The singularities along the lower holon line are also supported by a recent low energy theory [6]. For all parameter values we observe dominant weight along the above mentioned lines. For  $J/t = 0.4$ , we have checked that the results are consistent within the uncertainties of MEM with a peak along the edges and a further peak along

the holon lines, signaled by a broad structure between the edges and the holon lines (Fig. 2.a). We observed such a behaviour for  $0.33 \leq J/t \leq 0.6$ . For  $J/t \geq 1.2$  (Fig. 2.b and 2.c), the structure at the lower edge narrows considerably and the data are not any more consistent with an additional structure along the lower holon line for  $k < k_0$ , but only with a singularity for  $k > k_0$ . At  $J/t = 2$  the exact holon and spinon dispersions can be obtained by BA [15]. Figure 2.c shows the comparison with the CSSA, where on the one side the original dispersions are used (full line) and on the other side, with the dispersions as given by BA (crosses). Whereas the BA holon dispersion reproduces very well the lower edge, showing that as anticipated by the CSSA, at the SuSy point that edge is completely determined by the holon dispersion, the full bandwidth is better described with the original dispersions. We assign the additional weight in the region  $k > \pi/2$  to processes involving one holon and more than one BA spinon. In fact, that portion resembles the difference between the supports for one-holon/one-spinon and one-holon/three-spinon processes in the ISE model [7]. In our case, no limitation on the possible number of spinons exists, such that in principle all odd number of them are allowed. It is interesting to notice that using a fermionic spinon one is able to describe both the case  $J = 0$  and  $J = 2t$ . In the first case, the spinon in the exact solution is a fermion. At the SuSy point it is expected to be a semion [7,8] and on the basis of our results, we conclude that the fermionic spinon contains all possible states with an odd number of semionic spinons.

Finally, we consider the quasiparticle residue  $Z_k = \left| \langle \Psi_0^{L-1} | \tilde{c}_{k\sigma} | \Psi_0^L \rangle \right|^2$  at  $k = \pi/2$  for  $J = 2t$ .

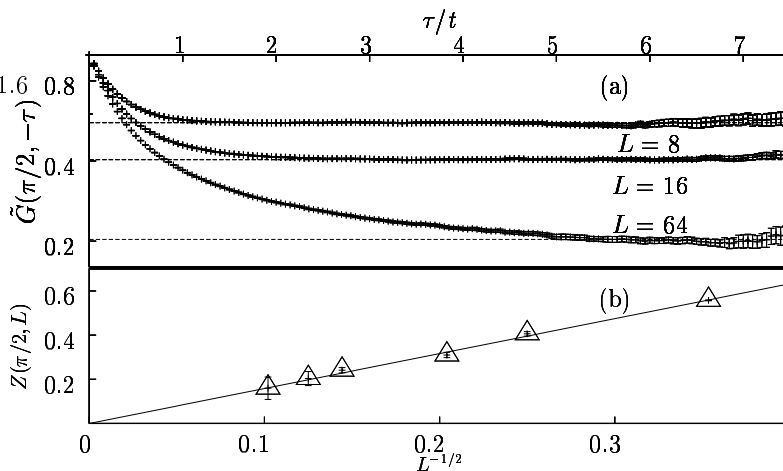


FIG. 3. Quasiparticle weight at  $k = \pi/2$ .

(a)  $\tilde{G}(\pi/2, -\tau) \equiv G(\pi/2, -\tau) \exp \left[ -\tau \left( E_0^L - E_0^{L-1}(\pi/2) \right) \right]$  versus  $\tau/t$ . At  $\tau/t \gg 1$  this quantity converges to the quasiparticle weight  $Z(\pi/2)$ . (b) Finite size scaling of  $Z(\pi/2)$  as obtained from (a). The solid line is a least square fit to the form  $L^{-1/2}$ . We consider  $\beta J = 30$  for  $L \leq 48$  and  $\beta J = 60$  for  $L > 48$ , to guarantee convergence in  $\tau$ .

As Fig. 2.c shows, the lower edge is very sharp and without prior knowledge, the question may arise whether we are dealing with a quasiparticle.  $Z_k$  is related to the imaginary time Green function through:

$$\lim_{\tau \rightarrow \infty} G(k, -\tau) \propto Z_k \exp \left[ \tau \left( E_0^L - E_0^{L-1}(k) \right) \right]. \quad (7)$$

Fig. 3.a shows  $G(\pi/2, -\tau) \exp \left( -\tau(E_0^L - E_0^{L-1}(\pi/2)) \right)$  versus  $\tau$ , where the energy difference is obtained by fitting the tail of  $G(\pi/2, -\tau)$  to a single exponential form, for several sizes. The thus estimated  $Z(\pi/2)$  is plotted versus system size in Fig. 3.b. Our results are consistent with a vanishing quasiparticle weight  $Z(\pi/2) \propto L^{-1/2}$  which is the scaling obtained by a combination of bosonization and conformal field theory [6]. Since the CPU-times scales as  $V\beta$  ( $V$  is the volume) the determination of the  $Z$ -factor may be efficiently extended to higher dimensions, in contrast to determinantal algorithms for the Hubbard model that scale as  $V^3\beta$ .

In summary, we have developed a new QMC algorithm which allows the determination of single-hole dynamics in quantum antiferromagnets. This algorithm is extremely powerful in the sense, that the required CPU time scales as  $V\beta$ . For the one dimensional case, we showed that the spectral function is well described by a simple model with free spinons and holons with dispersions given by  $J$  and  $2t$  respectively. The comparison of our results at the supersymmetric point lead to a characterization of the excitation content of the spectra for this particular parameter, where additional information is available from the Bethe *Ansatz* solution. Finally we computed the quasiparticle weight and showed that it vanishes as  $L^{-1/2}$ .

This work was supported by Sonderforschungsbereich 341 in Tübingen-Stuttgart. The numerical calculations were performed at HLRS Stuttgart and HLRZ Jülich. We thank the above institutions for their support.

- [1] C. Kim *et al*, Phys. Rev. Lett **77**, 4054 (1996).
- [2] K. Kobayashi *et al*, Phys. Rev. Lett **82**, 803 (1999).
- [3] T. Takahashi *et al.*, Phy. Rev. B **56**, 7870 (1997).
- [4] B.O. Wells *et al.*, Phys. Rev. Lett. **74**, 964 (1995).
- [5] S. Sorella and A. Parola, J. Phys. Condens. Matter **4**, 3589 (1992); K. Penc, F. Mila, and H. Shiba, Phys. Rev. Lett **75**, 894 (1995).
- [6] S. Sorella and A. Parola, Phys. Rev. Lett. **76**, 4604 (1996); Phys. Rev. B **57**, 6444 (1998).

- [7] Y. Kato, Phys. Rev. Lett **81**, 5402 (1998); Z. N. C. Ha and F. D. M. Haldane, Phys. Rev. Lett **73**, 2887 (1994);
- [8] F. D. M. Haldane, in *Correlation Effects in Low-Dimensional Electron Systems*, edited by A. Okiji and N. Kawakami (Springer Verlag, Berlin, 1994).
- [9] H. Suzuura and N. Nagaosa, Phys. Rev. B **56**, 3548 (1997).
- [10] G. Khaliullin, JETP Lett. **52**, 389 (1990); A. Angelucci, Phys. Rev. B **51**, 11580 (1995).
- [11] H. G. Evertz, M. Marcu, and G. Lana, Phys. Rev. Lett **70**, 875 (1993).
- [12] N. V. Prokof'ev, B. V. Svistunov, and I. S. Tupitsyn, JETP **87**, 310 (1998).
- [13] M. Jarrell and J. Gubernatis, Physics Reports **269**, 133 (1996); W. von der Linden, Applied Physics A **60**, 155 (1995).
- [14] P. W. Anderson, Science **235**, 1196 (1987); G. Baskaran and P. W. Anderson, Phys. Rev B **37**, 580 (1988).
- [15] P.-A. Bares and G. Blatter, Phys. Rev. Lett. **64**, 2567 (1990); P.-A. Bares, G. Blatter, and M. Ogata, Phys. Rev. B **44**, 130 (1991).